Improvement and Investigation of Electrostatic Comb Actuator Performance

Hao Sun , Yuxin Liu , Yu-Sheng Lin *

Posted Date: 19 December 2023

doi: 10.20944/preprints202312.1459.v1

Keywords: MEMS; electrostatic force; comb driver; stability; larger displacement; high performance

Article

Improvement and Investigation of Electrostatic Comb Actuator Performance

Hao Sun, Yuxin Liu and Yu-Sheng Lin *

School of Electronics and Information Technology, Sun Yat-Sen University, Guangzhou 510006, China
* Correspondence: linyoush@mail.sysu.edu.cn

Abstract: We present a design of electrostatic comb driver to improve and investigate its actuation performance. The proposed electrostatic comb actuator (ECA) is composed of two set of interdigitated comb microstructures, the inner combs are fixed to form the fish-bone microstructures and the outer combs are movable and connected to crab-leg flexure beams microstructures. The ECA is investigated to optimize the actuation performance by changing the comb shape and the intersection angle of crab-leg flexure beams. The comb shapes are compared between the traditional rectangle shape and the trapezoid shape, while the intersection angles of crab-leg flexure beams are compared between 45°, 60°, and 90° on the influences of ECA displacement and stability characteristics. These parameters are investigated for their impacts on the dynamic comb displacement and driving voltage. Under the condition of a driving DC bias voltage of 100 volts, the ECA displacement is firstly increased and then gradually decreased by increasing the comb finger length. The maximum displacement of ECA with trapezoid comb is 47.2 μm while that of ECA with rectangle comb is 22.4 μm. By using trapezoid comb shape to replace the rectangle comb under the same conditions, the ECA displacement is improved 2-fold. To enhance the stability of ECA system, the intersection angle of 90° of crab-leg flexure beams shows highest stability that is great better than the intersection angle of 45° and 60° of crab-leg flexure beams by increasing the driving different DC bias voltage to 100 volts on ECA. The stability of the ECA with the intersection angle of 90° of crab-leg flexure beams is enhanced 1.1-fold and 1.4-fold compared to that of 45° and 60° of crab-leg flexure beams, respectively. This design provides an optimized approach to the electrostatic comb actuator that can be used expansively in the gyroscope, motion sensor, position sensor, imaging sensor, optical sensor, and so on.

Keywords: MEMS; electrostatic force; comb driver; stability; larger displacement; high performance

1. Introduction

Micro-electro-mechanical systems (MEMS), also known as microsystems technology, is a technology that integrates mechanical and electronic components on a single chip and is manufactured using microfabrication techniques. The key components of MEMS include sensors, actuators, and microelectronics [1–3]. Microactuators are used to convert non-mechanical input energy into mechanical output energy. There are various types of microactuation technologies, with the most used being piezoelectric, magnetic, thermal, electrochemical, and electrostatic actuation [4–7]. Among these actuation mechanisms, electrostatic actuation is the most widely used driving technology. Electrostatic actuators do not require additional components such as coils or iron cores, and not rely on special materials like alloys or piezoelectric ceramics, which are not compatible to the standard CMOS manufacturing process. [8–16] It is less influenced by scaling and advantageous for the applications of ultra-large-scale integrated circuit transducer [17].

One of the most common electrostatic actuators is the comb-drive actuator. The comb-drive actuator consists of two interdigitated comb microstructures, one of which is fixed, and the other is connected to a flexible suspension microstructure. When applying a voltage difference between the comb microstructures, the movable comb microstructures can be actuated due to the electrostatic forces. The comb-drive actuator is widely utilized to achieve large displacement at low driving voltage. It was originally developed by Tang et al. in 1989 [18]. The applications of this comb-drive actuator are included but not limited to resonators [19–22], optical shutters [23], micro-mechanical

 doi:10.20944/preprints202312.1459.v1

gears [24,25], micro grippers [26,27], and micro tweezers [28]. This voltage-controlled comb-drive actuators are applied the lateral electrostatic forces to control the displacement of the movable comb teethes, making them attractive for micro-positioning applications in two-axis or three-axis micro-stages [29–31]. The advantages of using electrostatic comb-drive actuators are low power consumption, simplified electronic control, and easy sensing mechanism based on capacitance [32]. To achieve the above-mentioned merits, the stability of actuation system is a key role for high-performance actuator and sensor applications. The motion state of comb-driver can be restored by using spring microstructure to make the system stable, continuous, and reversible. Thus, the suspension microstructure is required to have a lower spring constant in the desired displacement direction and a higher spring constant in the vertical direction. The electrostatic force increases along with an increment of the number of comb fingers and a decrement of the gap between them. In addition to these parameters, the length of the suspension microstructure is also a variable to achieve larger displacement at lower driving voltage.

In view of above points, we present a design of electrostatic comb actuator (ECA) to improve and investigate its actuation performance. The proposed ECA is composed of two set of interdigitated comb microstructures, the inner combs are fixed to form the fish-bone microstructures and the outer combs are movable and connected to crab-leg flexure beams microstructures. This study aims to achieve larger displacements at lower driving voltage by varying different design parameters. The working principle is initially discussed, followed by an exploration of the impact of different comb shapes and the intersection angles of crab-leg flexure beams on system performance.

2. Design and Method

Figure 1(a) shows the schematic diagram of the proposed ECA. The configurations of comb fingers are illustrated in Figure 1(b), which are compared between the rectangular and trapezoidal comb shapes including the relative geometric parameters. The variable l and g parameters represent the comb finger length and the overlap between comb fingers, respectively. The space between comb fingers is 40 μm, and the linewidth of the rectangular combs is 15 μm. For trapezoidal combs, the bottom linewidth is 20 μm, and the top linewidth is 15 μm. Figure 1(c) illustrates the parameters of the crab-leg flexure beams. The beam length is 1200 μm, the space between adjacent crab-leg flexure beams is 10 μm, and the space between crab-leg flexure beam groups is 200 μm. The variable parameter is the intersection angles of crab-leg flexure beams, which is defined as θ. Thus, the impacts of different l, g values, and crab-leg flexure beams angles are compared and discussed as θ = 45°, 60°, and 90°. Figure 1(d) illustrates the fabrication process flow of the proposed ECA. First, a silicon-on-insulator (SOI) wafer is prepared and cleaned. The thicknesses of device layer, insulation layer, and handle layer are 50 μm, 1 μm, and 300 μm, respectively. Second, the pattern of ECA is defined by using maskless photolithography process. Third, the microstructures of ECA including fishbone combs and crab-leg flexure beams are etched by using deep reactive ion etching (DRIE) process. Finally, the microstructures of ECA are released by using vapor hydrogen fluoride (VHF) to make the ECA microstructures suspension.

Preprints (www.preprints.org) | NOT PEER-REVIEWED | Posted: 19 December 2023 doi:10.20944/preprints202312.1459.v1

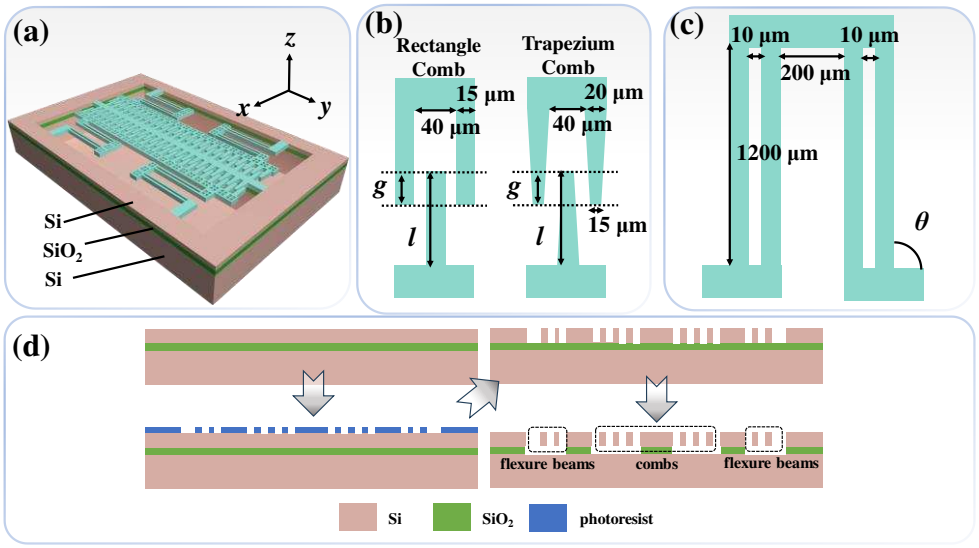

Figure 1. Schematic drawings of (a) the proposed ECA with (b) rectangle and trapezium combs, and (c) crab-leg flexure beams geometry. (d) The fabrication process flow of the proposed ECA.

The proposed ECA is driven by electrostatic force generated from the voltage difference applied between the fixed and movable combs. The operation mechanism of the ECA is based on the force balance between the electrostatic force and the mechanical restoring force generated by the crab-leg flexure beams. The driving voltage is applied to the movable combs and the fixed combs are anchored and connected to grounding electrode. The applied voltage difference between the combs leads to the deflection of the movable comb fingers caused from the generation of electrostatic force. This electrostatic force provides an actuation in the movable direction of the comb fingers. This displacement results in a change in the overlapping area, thereby causing a variation in the capacitance value. The position of the movable comb finger is controlled by a balance between the electrostatic force and the mechanical restoring force of the crab-leg flexure beams. The change in capacitance is given by the following equation [31].

$$\Delta C = \frac{N\varepsilon_0 t(\Delta x+g)}{w} \quad (1)$$

where Δx represents the displacement of the movable combs, N is the number of comb finger, ε_0 is relative dielectric constant, w is space between comb fingers, t is time, and g is the interdigitated distance between the comb fingers. The electrostatic force in the x-axis direction is given by the following equation.

$$F_e = \frac{N\varepsilon_0 t}{2w}V^2 \quad (2)$$

where V is the driving bias voltage. The displacement of the movable comb finger (x) equals electrostatic force (F_e) divided by the mechanical stiffness constant of the the crab-leg flexure beams (K), i.e., $x = F_e/K$. K can be expressed by

$$K = 2Et\left(\frac{W_c}{l}\right)^3 \quad (3)$$

where E is the electric field intensity, l is the comb finger length, and W_c is the equivalent comb finger width. Therefore, the displacement is given by the following equation.

$$x = \frac{N\varepsilon_0 V^2}{4Ew}\left(\frac{l}{W_c}\right)^3 \quad (4)$$

It is because that the structural material of ECA is silicon, which shows excellent mechanical and electrical properties, and can be further modified through doping [2]. In this study, the properties of the used silicon material are Young's modulus of 160 GPa, Poisson ratio of 0.22, density of 2320 kg/m^3, and dielectric constant of 4.5, respectively.

Preprints (www.preprints.org) | NOT PEER-REVIEWED | Posted: 19 December 2023 doi:10.20944/preprints202312.1459.v1

3. Results and Discussions

Figure 2 shows relationships of displacements and ECA with different comb finger lengths under a driving DC bias voltage of 100 volts. Figure 2(a) and (b) represent the comb finger with rectangular and trapezoidal shapes, respectively. It can be observed that for both rectangular and trapezoidal comb shapes, the displacement of the combs shows a trend of initially increasing and then decreasing along with the increment of the comb finger length. According to Eq. (4), the displacement of the comb finger is related to the comb finger length (l), the electric field intensity (E), and the driving bias voltage (V). When the driving bias voltage (V) keeps as constant, the electric field intensity (E) will be increased along with the increment of the comb finger length (l). Initially, the influence of the comb finger length is dominant that the comb finger displacement will be gradually increased. However, as the influence of the electric field intensity becomes dominant that the comb finger displacement is gradually decreased. Additionally, the different comb shape such as rectangle and trapezoid, has different equivalent comb finger width (W_c), which will result in the variations of the turning points in the displacement.

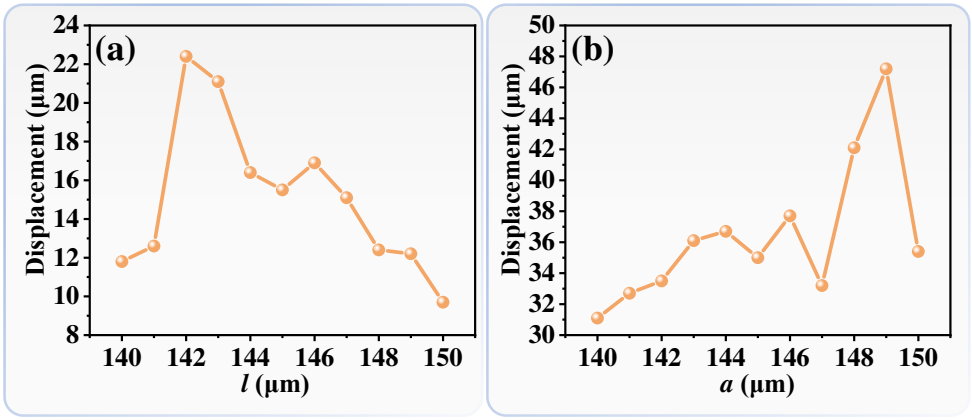

Figure 2. Relationships of displacements and ECA with different comb finger lengths under a driving DC bias voltage of 100 volts. The comb fingers are (a) rectangle and (b) trapezium shapes.

To further investigate the influence of different crab-leg flexure beam configurations on the stability of ECA, Figure 3 shows the relationships of comb fingers displacements and driving bias voltages for ECA crab-leg flexure beams with different θ values (45°, 60°, and 90°), while keeping the comb finger length (l) as constant as 149 μm. Figure 3(a) and (b) represent the comb finger with rectangle and trapezoid shape, respectively. The trend of comb fingers displacements and bias voltages exhibits a quadratic relationship, which is consistent with the Eq. (4). As the intersection angle of crab-leg flexure beams decreases, the displacement of the ECA increases under the same DC bias voltage. When the ECA with rectangle combs is applied a driving DC bias voltage of 100 volts, the displacements are 52.36 μm, 19.95 μm, and 12.15 μm for θ = 45°, 60°, and 90°, respectively. The displacement of crab-leg flexure beams with θ = 45° is 2.6-fold and 4.3-fold compared to that with θ = 60° and θ = 90°, respectively. While the ECA with trapezoid combs is applied a driving DC bias voltage of 100 volts, the displacements are 159.69 μm, 70.71 μm, and 47.12 μm for θ = 45°, 60°, and 90°, respectively. The displacement of crab-leg flexure beams with θ = 45° is 2.3-fold and 3.4-fold compared to that with θ = 60° and θ = 90°, respectively. To compare the ECA with trapezoid combs to that with rectangle combs, the displacements are enhanced 3.9-fold for θ = 90°, 3.5-fold for θ = 60°, and 3.0-fold for θ = 45°, respectively. The ECA with trapezoid combs exhibits significantly larger displacement compared to the ECA with rectangle combs. When the ECA with rectangle combs and θ = 45° is applied a DC bias voltage of 65 volts, the displacement of the ECA deviates from the quadratic trend. It is attributed to the structural instability of the ECA with θ = 45°. Thus, to further investigate the relationships between ECA stabilities and crab-leg flexure beams angles in detail, the displacements along x- and y-axis are analyzed and discussed sequentially. That will impact the overall performance and reliability of the ECA device.

Preprints (www.preprints.org) | NOT PEER-REVIEWED | Posted: 19 December 2023 doi:10.20944/preprints202312.1459.v1

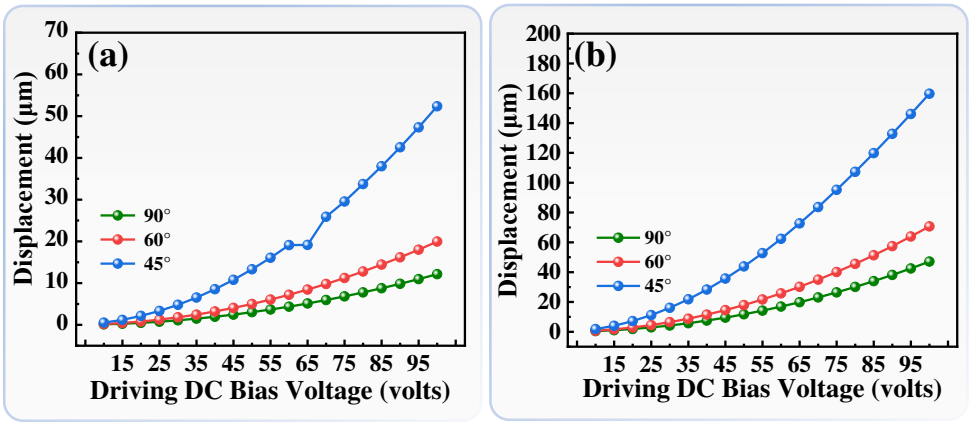

Figure 3. Relationships of comb fingers displacements and driving bias voltages for ECA crab-leg flexure beams with different θ values, where the comb finger length (l) is kept as constant as 149 μm. The comb fingers are (a) rectangle and (b) trapezium shapes.

To better illustrate the influences of crab-leg flexure beams angles on the stability of the ECA, the energy field distributions of the ECA with rectangle and trapezoid combs along the *x*-, *y*-, and *z*-axis directions are plotted in Figure 4. The driving DC bias voltage is kept as constant as 100 volts. Figure 4(a) and (b) show the ECA with rectangle and trapezoid combs under the condition of $\theta = 90°$, respectively. The ECA with rectangle combs exhibits maximum displacements of 12.8 μm in the *x*-axis direction, 0.17 μm in the *y*-axis direction, and 1.26 μm in the *z*-axis direction. The maximum displacement of the ECA with rectangle combs in the *x*-axis direction is 75.3-fold larger than that in the *y*-axis direction and 10.16-fold larger than that in the *z*-axis direction. While the ECA with trapezoid combs exhibits maximum displacements of 48.1 μm in the *x*-axis direction, 0.57 μm in the *y*-axis direction, and 1.05 μm in the *z*-axis direction. Here, the maximum displacement of the ECA with trapezoid combs in the *x*-axis direction is 84.4-fold larger than that in the *y*-axis direction and 45.8-fold larger than that in the *z*-axis direction. Figure 4(c) and (d) show the ECA with rectangle and trapezoid combs under the condition of $\theta = 60°$, respectively. The ECA with rectangle combs exhibits maximum displacements of 21.7 μm in the *x*-axis direction, 5.03 μm in the *y*-axis direction, and 7.19 μm in the *z*-axis direction. The maximum displacement of the ECA with rectangle combs in the *x*-axis direction is 4.3-fold larger than that in the *y*-axis direction and 3.0-fold larger than that in the *z*-axis direction. While the ECA with trapezoid combs exhibits maximum displacements of 72.3 μm in the *x*-axis direction, 17.6 μm in the *y*-axis direction, and 2.93 μm in the *z*-axis direction. The maximum displacement of the ECA with trapezoid combs in the *x*-axis direction is 4.1-fold larger than that in the *y*-axis direction and 24.7-fold larger than that in the *z*-axis direction. Figure 4(e) and (f) show the ECA with rectangle and trapezoid combs under the condition of $\theta = 45°$, respectively. The ECA with rectangle combs exhibits maximum displacements of 57.5 μm in the *x*-axis direction, 29.5 μm in the *y*-axis direction, and 19.0 μm in the *z*-axis direction. The maximum displacement of the ECA with rectangle combs in the *x*-axis direction is 1.9-fold larger than that in the *y*-axis direction and 3.0-fold larger than that in the *z*-axis direction. While the ECA with trapezoid combs exhibits maximum displacements of 161 μm in the *x*-axis direction, 99.1 μm in the *y*-axis direction, and 5.43 μm in the *z*-axis direction. The maximum displacement of the ECA with trapezoid combs in the *x*-axis direction is 1.6-fold larger than that in the *y*-axis direction and 29.7-fold larger than that in the *z*-axis direction. The higher stability of the ECA is defined by the greater difference between the displacements in the *x*-axis direction and the *y*/*z*-axis directions. When $\theta = 90°$, the ECA exhibits the best stability. Conversely, when $\theta = 45°$, the stability of the ECA is the worst. Moreover, for the same crab-leg flexure beams angle, the ECA with trapezoid combs exhibits slightly better stability compared to that with rectangle combs. This suggests that the ECA with trapezoid combs possesses advantages of larger displacement and better stability compared to that with rectangle combs.

Preprints (www.preprints.org) | NOT PEER-REVIEWED | Posted: 19 December 2023 doi:10.20944/preprints202312.1459.v1

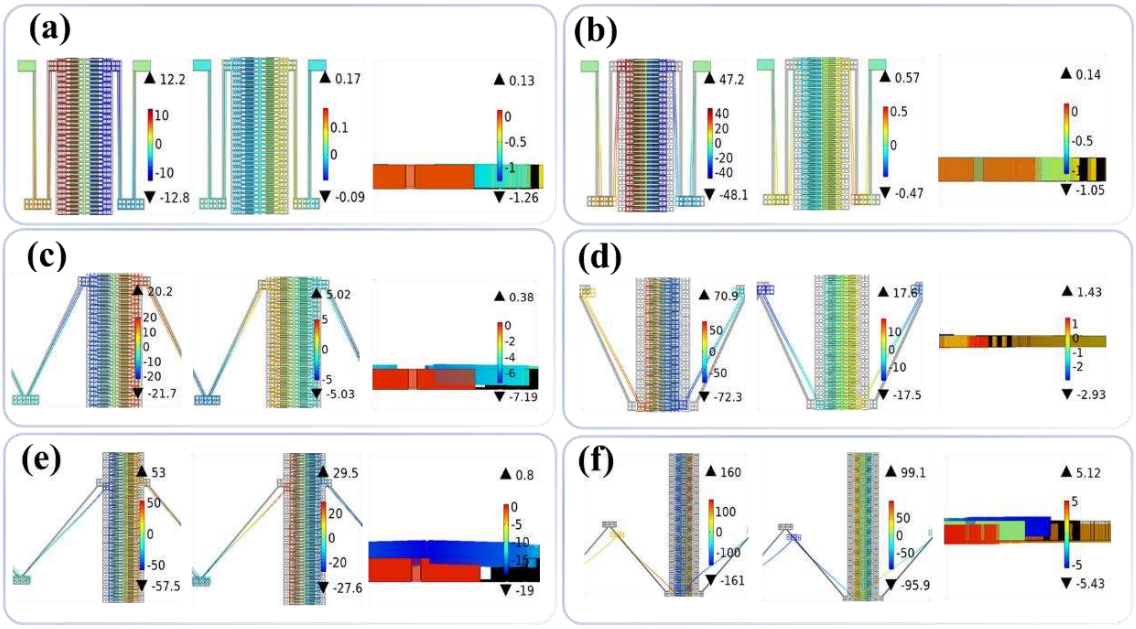

Figure 4. Energy field distributions of the ECA with (a)(b) $\theta = 90°$, (c)(d) $\theta = 60°$, and (e)(f) $\theta = 45°$ in x-, y-, and z-axis directions, respectively. The comb fingers are (a)(c)(e) rectangle and (b)(d)(f) trapezoid shapes and the driving DC bias voltage is kept as constant as100 volts.

The relationships of displacements and different driving DC bias voltages of ECA with trapezoid combs under the conditions of $\theta = 90°$, 60°, and 45° are summarized in Figure 5(a-c), respectively. In Figure 5(a), when $\theta = 90°$, the trends of displacements and driving DC bias voltages in the x-axis direction exhibits a quadratic relationship. At a DC bias voltage of 100 volts, the displacement in the x-axis direction is 44 μm, and the displacement in the y-axis direction is only 0.36 μm. This demonstrates that the ECA with trapezoid combs and $\theta = 90°$ possesses high stability and large displacement. In Figure 5(b), when $\theta = 60°$, although the displacement in the x-axis direction increases to 64.89 μm at a DC bias voltage of 100 volts, however, the displacement in the y-axis direction also increases to 5.58 μm. It indicates that the ECA starts to be unstable by reducing the crab-leg flexure beams angle. When $\theta = 45°$, the displacement in the x-axis direction has a significant increase, which reaches up to 150.47 μm at a DC bias voltage of 100 volts as shown in Figure 5(c). However, the displacement in the y-axis direction also increases to 44.552 μm. It indicates that the ECA is highly unstable. The relationships of stabilities and different driving DC bias voltages under the conditions of different crab-leg flexure beams angles are summarized in Figure 5(d). The stability of ECA is defined as the difference between the ratio of the displacement in the y-axis direction to the displacement in the x-axis direction and unity. When $\theta = 90°$, the stability of the ECA exceeds 0.99 from the driving DC bias voltage of 20 volts to 100 volts. While $\theta = 60°$, the stability of the ECA decreases from 0.92 at driving DC bias voltage of 20 volts to 0.91 at driving DC bias voltage of 100 volts. It maintains above 0.90. When $\theta = 45°$, the stability of the ECA drops to 0.81 at driving DC bias voltage of 20 volts and further diminishes to 0.7 at driving DC bias voltage of 100 volts. Under a DC bias voltage of 100 volts, the stability of the ECA with $\theta = 90°$ is 1.1-fold higher than that with $\theta = 60°$ and 1.4-fold higher than that $\theta = 45°$, respectively. These results indicate that the optimized design of ECA with trapezoid combs and crab-leg flexure beams of 90° exhibits larger displacement and stability.

Preprints (www.preprints.org) | NOT PEER-REVIEWED | Posted: 19 December 2023 doi:10.20944/preprints202312.1459.v1

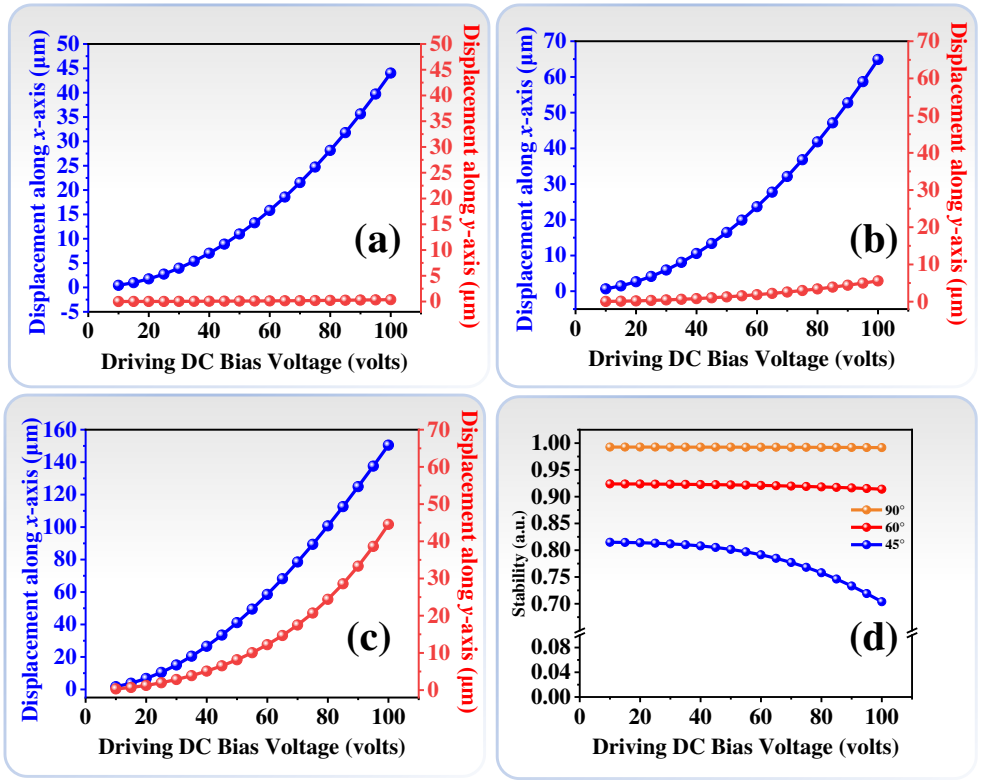

Figure 5. Relationships of displacements and different driving DC bias voltages under the conditions of (a) $\theta = 90°$, (b) $\theta = 60°$, and (c) $\theta = 45°$, (d) Relationships of stability and different driving DC bias voltages under the conditions of different crab-leg flexure beams angles.

4. Conclusion

In conclusion, we present a design of optimized ECA with trapezium combs. The comparisons of ECA with traditional rectangle shape and the trapezoid shape and the intersection angles of crab-leg flexure beams are compared on the influences of ECA displacement and stability characteristics. By using the trapezoid comb shape, the displacement of ECA can be improved 2-fold larger than that used rectangle comb shape. It is attributed to the combined effect of electric field intensity and the strength of trapezoid comb fingers are higher than those of rectangle comb fingers. Moreover, we also analyse the intersection angles of crab-leg flexure beams on the influences of ECA displacement and stability characteristics. When $\theta = 45°$, the displacement is larger 2.3-fold and 3.4-fold compared to that of $\theta = 60°$ and $\theta = 90°$, respectively, but the ECA system is unstable. When $\theta = 90°$, the stability of ECA system is 0.99 under the driving voltage of 100 volts, which is enhanced 1.1-fold and 1.4-fold stabler than that of $\theta = 45°$ and $\theta = 60°$, respectively. In this study, the design of ECA with trapezoid combs can enhance the system displacement and the design of the intersection angle of 90° of crab-leg flexure beams can improve the stability of ECA system. Such approach opens an avenue for the expansive sensing applications of ECA in the motion, position, imaging, biomedical, optical fields.

Funding: Guangzhou Basic and Applied Basic Research Project (202201011829).

Acknowledgments: The authors acknowledge the State Key Laboratory of Optoelectronic Materials and Technologies of Sun Yat-Sen University for the use of experimental equipment.

Conflicts of Interest: The authors declare no conflicts of interest.

References

1. S. Beeby, G. Ensell, M. Kraft and N. White, MEMS Mechanical Sensors, Artech, (2004).
2. T. Kan, A. Isozaki, N. Kanda, N. Nemoto, K. Konishi, H. Takahashi, M. Kuwata-Gonokami, K. Matsumoto and I. Shimoyama, Enantiomeric switching of chiral metamaterial for terahertz polarization modulation employing vertically deformable MEMS spirals, Nat. Commun, **6**, 8422 (2015).
3. S. V. Hum and J. Perruisseau-Carrier, Reconfigurable Reflectarrays and Array Lenses for Dynamic Antenna Beam Control: A Review, IEEE Trans. Antennas Propag, **62**(1), 183-198 (2014).
4. Z. He, G. Guo, L. Feng, W. E. Wong and H. T. Loh, Microactuation mechanism with piezoelectric element for magnetic recording head positioning for spin stand, Proc Inst Mech Eng C J Mech Eng Sci, **220**(9), 1455-1461 (2006).
5. C. R. Friedrich, J. Fang and R. O. Warrington, Micromechatronics and the miniaturization of structures, devices, and systems, IEEE Trans Compon Packaging Manuf Technol, **20**(1), 31-38 (1997).
6. R. H. Wolf and A. H. Heuer, TiNi (shape memory) films silicon for MEMS applications, J Microelectromech Syst, **4**(4), 206-212 (1995).
7. Tong Daqun, R. L. Williams and S. K. Agrawal, Optimal shape control of composite thin plates with piezoelectric actuators, J Intell Mater Syst Struct, **9**(6), 458-467 (1998).
8. C. I. Lee, C. H. Ko, T. C. Huang and F. C. Hsu, Multiactuation complementary metal-oxide semiconductor radio frequency MEMS switch, J Micro Nanolithogr MEMS MOEMS, **9**(3), 033008 (2010).
9. Chiung-I Lee, Chih-Hsiang Ko and Tsun-Che Huang, A novel multi-actuation CMOS RF MEMS switch, Proceedings of the SPIE - The International Society for Optical Engineering, **7268**, 726804 (2008).
10. J. C. Chiou and C. F. Kuo, Development of vertical electrostatic comb-drive actuator using magnified cascade configuration, Jpn J Appl Phys, **46**(10A), 6546-6549 (2007).
11. Z. X. Cheng and H. Toshiyoshi, CMOS-MEMS Micro-Mirror Arrays by Post-Processing ASMC 0.35-μm CMOS Chips, J Microelectromech Syst, **26**(6), 1435-1441 (2017).
12. K. U. Harms and J. T. Horstmann, Fabrication concept for a CMOS-compatible electrostatically driven surface MEMS switch for RF applications, Microelectron Eng, **73-74**, 468-473 (2004).
13. Y. Okamoto and Y. Mita, Integrated 0-30 V switching driver circuit fabricated by mesa isolation postprocess of standard 5 V CMOS LSI for MEMS actuator applications, Microsyst. Technol., **24**(1), 503-510 (2018).
14. S. P. Mahmoudi and A. Mahmoudi, An electrothermally-driven low voltage micro switch for high frequency application, J. Electr., **14**(2), 6 (2014).
15. H. Takao, T. Ichikawa, T. Nakata, K. Sawada and M. Ishida, A Versatile Integration Technology of SOI-MEMS/CMOS Devices Using Microbridge Interconnection Structures, J Microelectromech Syst, **19**(4), 919-926 (2010).
16. A. H. Alameh and F. Nabki, A 0.13-µm CMOS Dynamically Reconfigurable Charge Pump for Electrostatic MEMS Actuation, IEEE Trans Very Large Scale Integr VLSI Syst, **25**(4), 1261-1270 (2017).
17. R. Legtenberg, A W Groeneveld and M Elwenspoek, Comb-drive actuators for large displacements, J Micromech Microeng, 6(3), 320 (1996).
18. W. C. Tang, T.-C. H. Nguyen and R. T. Howe, Laterally driven polysilicon resonant microstructures, Sens. Actuators B Chem, **20**, 25-32 (1989).
19. Brennen, A. Reid, P. Pisano Albert and W.-C. Tang, Multiple mode micromechanical resonators, IEEE Proceedings on Micro Electro Mechanical Systems, An Investigation of Micro Structures, Sensors, Actuators, Machines and Robots, 9-14 (1990).

20. G. J. Verbiest, D. Xu, M. Goldsche, T. Khodkov, S. Barzanjeh, N. von den Driesch, D. Buca and C. Stampfer, Tunable mechanical coupling between driven microelectromechanical resonators, Appl. Phys. Lett, 109(14), 143507 (2016).
21. Y. Xie, J. Lee, Y. N. Wang and P. X. L. Feng, Straining and Tuning Atomic Layer Nanoelectromechanical Resonators via Comb-Drive MEMS Actuators, Adv. Mater, 6(2), 2000794 (2021).
22. R. R. A. Syms and D. F. Moore, Focused ion beam tuning of in-plane vibrating micromechanical resonators, Electron. Lett., **35**(15), 1277-1278 (1999).
23. Y. J. Lai, E. V. Bordatchev, S. K. Nikumb and W. Y. Hsu, Performance characterization of in-plane electro-thermally driven linear microactuators, J Intell Mater Syst Struct, **17**(10), 919-929 (2006).
24. L. A. Romero, F. M. Dickey and S. C. Holswade, A method for achieving constant rotation rates in a microorthogonal linkage system, J Microelectromech Syst, **9**(2), 236-244 (2000).
25. A . Albers, N. Burkardt and J. Marz, Restrictions in the design of gear wheel components and drives for micro technology, Microsyst. Technol., **9**(3), 192-196 (2003).
26. B. S. Kim, J. S. Park, B. H. Kang and C. Moon, Fabrication and property analysis of a MEMS micro-gripper for robotic micro-manipulation, Robot Cim-int Manuf., **28**(1), 50-56 (2012).
27. S. E. Nashat, R. AbdelRassoul and A. E. Abd El Bary, Design and simulation of RF MEMS comb drive with ultra-low pull-in voltage and maximum displacement, Microsyst. Technol., **24**(8), 3443-3453 (2018).
28. H. L. Kang and L. Z. Xu, Forces on magnetic-driven micro-tweezers based on micro-four-link mechanism, Mech. Based Des. Struct. Mach., **51**(2), 706-720 (2023).
29. K. Laszczyk, S. Bargiel, C. Gorecki, J. Krezel, P. Dziuban, M. Kujawinska, D. Callet and S. Frank, A two directional electrostatic comb-drive X-Y micro-stage for MOEMS applications, Sens. Actuator A Phys., **163**(1), 255-265 (2010).
30. J. C. Lee and D. W. Lee, Fabrication of a micro XY-stage using SU-8 thermal actuators, Microelectron Eng., **86**(4-6), 1267-1270 (2009).
31. Y. S. Choi, Y. Zhang and D. W. Lee, A thermal-driven silicon micro xy-stage integrated with piezoresistive sensors for nano-positioning, J. Micromech Microeng, **22**(5), 055002 (2012).
32. J. C. Wang, W. B. Rong, L. N. Sun and X. X. Li, Single Neuron Adaptive PID Control of the Silicon-based Integrated Micro Nano-Positioning XY-Stage, Adv. Mater. Res, **60-61**, 207 (2009).